Journal of Catalysis **192,** 286–295 (2000)
doi:10.1006/jcat.2000.2851, available online at http://www.idealibrary.com on IDEAL®

Structure and Catalytic Properties of Dimeric Copper(II) Acetato Complexes Encapsulated in Zeolite-Y

S. Chavan, D. Srinivas, and P. Ratnasamy[1]

National Chemical Laboratory, Pune, Maharashtra 411 008, India

Received September 1, 1999; revised February 4, 2000; accepted February 21, 2000

Dimeric copper acetate and chloroacetate complexes (CuAc and CuClAc, respectively), were encapsulated in zeolite-Y by the flexible ligand synthesis method. Spectroscopic techniques (FT-IR, diffuse reflectance UV–visible, and EPR) and thermal analysis provide convincing evidence for the formation of acetato-bridged dimeric copper(II) complexes in the supercages of zeolite-Y. The effects of encapsulation on the geometric, magnetic, spectral, and catalytic properties are examined. The separation ($\Delta\nu$) between $\nu_{as}(COO^-)$ and $\nu_s(COO^-)$ bands in the FT-IR spectra changes from 182 to 213 cm^{-1} for CuAc and 185 to 205 cm^{-1} for CuClAc upon encapsulation and corresponds to the *syn–syn* mode of coordination for the bridging carboxylato groups. Variable temperature EPR studies (77–298 K) indicate an antiferromagnetic interaction between the two Cu(II) ions in the dimers. The magnitude of the exchange interaction between the two Cu(II) ions and molecular symmetry for both the complexes change as a consequence of encapsulation. The Cu–Cu separation in the dimer decreases upon encapsulation, from 2.64 to 2.40 Å for CuAc and from 2.92 to 2.73 Å for CuClAc. The complexes catalyze the *o*-hydroxylation of phenols to catechols and additional oxidation to *o*-benzoquinone by molecular oxygen. The turnover frequency for phenol conversion increases significantly upon encapsulation. Due to the enhanced Cu–Cu binding upon encapsulation, the strength and lability of the Cu–phenolate and Cu-dioxygen bonds are modified by a trans-axial ligand effect accounting for the enhanced reactivity of the encapsulated complex.

Key Words: copper acetate; copper chloroacetate; oxidation; hydroxylation; zeolite catalysts; electron paramagnetic resonance; structure-activity correlation; enzyme mimic; oxygenase; tyrosinase; zeozyme.

INTRODUCTION

Transition metal complexes encapsulated in the cavities of zeolites and mesoporous materials show enhanced catalytic activity, compared to the "neat" complexes (1–10). We had found earlier that copper(II) acetate exhibited enhanced regioselective *o*-hydroxylation of L-tyrosine to L-dopa on encapsulation in molecular sieves Y, MCM-22, and VPI-5 using atmospheric oxygen as the oxidant (11). Subsequently, similar results were also reported by Rao *et al.* for Cu(II) acetate encapsulated in cubic Al–MCM-48 (12). Why do the intrinsic catalytic activities (turnover frequencies) of such complexes increase upon encapsulation in zeolites? In the present study, we probe the origin of the enhancement in the oxidation activity of copper acetates upon encapsulation in zeolites, using FT-IR, UV–vis, and especially EPR spectroscopy.

The single-crystal X-ray crystal structure of copper acetate monohydrate (13, 14) revealed the presence of isolated dimeric units in the solid state with an unusually short Cu–Cu separation of 2.61 Å (which is only slightly longer than the separation in copper metal, i.e., 2.54 Å). Dimeric copper ions form the active centers of many copper proteins for multielectron redox processes and oxygen activation (15, 16). Further, the carboxylato group acts as a bridging unit in several metalloproteins, e.g., hemerythrin, Mn catalases, etc. The EPR spectroscopy is well suited for the study of changes in the molecular structure of copper acetate dimers upon encapsulation in zeolites. EPR spectroscopy can not only distinguish between the monomeric and dimeric forms but also throw light on the structural changes that occur upon encapsulation as well as their preferred molecular conformations in the zeolite cavities. The latter information is crucial in exploring the reasons for the enhanced reactivity of the copper acetate complexes upon encapsulation. To our knowledge, this is the first detailed EPR study of encapsulated dimeric copper acetate complexes in zeolites.

EXPERIMENTAL

Materials

Cu–H-Y. Copper-exchanged zeolite-Y (Cu–H-Y) was prepared by ion exchange of zeolite H-Y with Cu(II) ions. To 3.5 g of H-Y zeolite was added 1.8 g of copper acetate monohydrate (Aldrich Co.) dissolved in 20 ml of distilled water. The mixture was stirred gently at 323 K for a

[1] To whom correspondence should be addressed. E-mail: prs@ems.ncl.res.in. Fax: (91)-20-5893355.

0021-9517/00 $35.00

period of 3–4 h. The sky-blue biphasic system was now aged overnight, after which it was filtered off. Cu–H-Y, thus prepared, was washed with warm, distilled water until the extract contained no copper ions. The solid was dried at 373 K in a static air oven for 8 h. The above exchange procedure was repeated twice. The sky-blue Cu–H-Y sample was stored in a dry desiccator containing $CaCl_2$. The amount of copper loading was estimated to be 0.11 wt% by atomic absorption spectrometry. Spectral studies revealed that the copper in these samples is present as exchangeable cations.

"Neat" $Cu(CH_3COO)_2$ and $Cu(CH_2ClCOO)_2$. Commercial quality $Cu(CH_3COO)_2 \cdot H_2O$ obtained from LOBA Chem., India was used as received. $Cu(CH_2ClCOO)_2 \cdot 2.5H_2O$ was prepared by neutralizing an aqueous solution (10 ml) of chloroacetic acid (1.89 g) with NaOH (0.82 g) in 5 ml of distilled water. An aqueous solution (10 ml) of $CuCl_2 \cdot 2H_2O$ (1.71 g) was then added dropwise and the resulting mixture was refluxed for 2 h. Good quality single crystals (greenish-blue) were obtained upon slow evaporation at room temperature for 5 days. The purity of the acetate complexes was checked by elemental analysis. Anal. Calcd. for $Cu(CH_3COO)_2 \cdot H_2O$: C, 24.06%, H, 4.01%. Found: C, 23.91%, H, 4.09%. Anal. Calcd. for $Cu(CH_2ClCOO)_2 \cdot 2.5H_2O$: C, 17.88%; H, 2.23%. Found: C, 16.53%; H, 2.08.

$Cu(CH_3COO)_2$ and $Cu(CH_2ClCOO)_2$ encapsulated in H-Y. The zeolite encapsulated copper acetate and chloroacetate complexes (CuAc-Y and CuClAc-Y, respectively) were prepared as follows: Cu–H-Y (3.5 g) was evacuated at 383 K for 2 h and then exposed to the vapours of acetic acid or monochloroacetic acid in a BET adsorption apparatus at 333 and 353 K, respectively, for 90 min, until the colour of the zeolite changed from sky-blue to bluish green. The materials were stored in a dry desiccator containing $CaCl_2$.

Procedures

Chemical analysis was done using a Hitachi (Z 8000) atomic absorption spectrometer. Carbon and hydrogen were estimated using a Carlo Erba EA 1108 elemental analyser. X-ray diffractograms for powder samples of H-Y, Cu–H-Y, and encapsulated metal complexes were recorded on a Rigaku RINT 2000 series X-ray diffractometer with a Cu$K\alpha$ radiation (40 kV, 150 mA) at 0.1° step size and 0.27°/s scan speed over the range $5° < 2\theta < 50°$. The samples were prepared as thin layers on metal or glass slides. Thermogravimetric and differential thermal analyses (TGA and DTA) were performed on an automatic derivatograph (Setaram TG-DTA 92).

FT-IR spectra of solids were recorded on a Shimadzu FT-COM 1 spectrophotometer as nujol mulls. The diffuse reflectance UV–visible spectra (DRS UV–vis) of the solid catalysts were recorded using a UV-101 PC scanning spectrophotometer. EPR spectra of the solid catalysts were recorded on a Bruker EMX spectrometer operating at X-band frequency and 100-kHz field modulation. Frequency calibration was done using a frequency counter fitted in a ER 041 XG-D microwave bridge. DPPH was used a field marker. Variable temperature experiments, in the range 80–380 K, were performed using a Bruker BVT 3000 temperature controller and the spectra at 77 K were measured using a quartz finger Dewar (Bruker ER 167 FDS-Q). Spectral simulations and manipulations were carried out using Bruker Simfonia and WINEPR software packages.

Catalytic Activity—Hydroxylation of Phenol

Phenol (1.88 g) and catalyst (0.073 g) in a 20-ml phosphate buffer (pH 6.5) were taken in a double-necked 100-ml glass reactor equipped with a water-cooled condenser, magnetic stirring rod, and rubber septum. The reactions were carried out in phosphate buffer (pH 6.5) as the dimeric structure of the complexes is stable only at this pH. The hydoxylation reactions were carried out at 298 K. Molecular oxygen (1 atm) was passed continuously through the reaction mixture. After 19 h, the solid catalyst was separated by centrifuging. The supernant liquid containing the products was extracted with diethyl ether. The products in the organic layer were analysed by a Shimadzu GC 14-B gas chromatograph equipped with a SE 52 chromatographic column (2-m long and 0.125-in. diameter) and a flame ionization detector. No indication of copper leaching into the reaction mixture was noticed. The amount of catalyst was chosen such that the molar concentration of copper was similar in all the experiments. Turnover frequencies (TOF) for the "neat" and encapsulated complexes were determined based on the dimeric Cu content. No products of the hydroxylation reaction were observed over Cu–H-Y.

RESULTS AND DISCUSSION

No major changes were observed in the X-ray diffraction patterns of zeolite H-Y upon formation and encapsulation of acetato and chloroacetato Cu(II) complexes, indicating that encapsulation of the complexes did not alter the framework structure of zeolite-Y.

Thermogravimetric Analysis

A comparative thermogravimetric analysis of copper-*exchanged* zeolite-Y (Cu–H-Y), "neat" copper complexes (CuAc and CuClAc), and *encapsulated* complexes (CuAc-Y and CuClAc-Y) in flowing dry air showed weight losses due to the decomposition of water and acetato or chloroacetato molecules. Representative TGA and DTA profiles of CuAc-Y and CuClAc-Y are shown in Fig. 1. The several stages of *endothermic* weight losses in the temperature

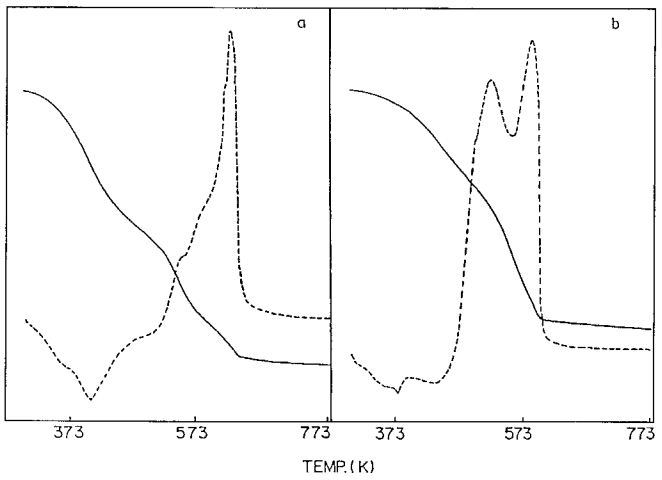

FIG. 1. TGA (—) and DTA (---) profiles of (a) CuAc-Y and (b) CuClAc-Y.

range 313–493 K correspond to the desorption of condensed, physically adsorbed and chemisorbed (in the form of OH groups) water, in the zeolite channels and cavities as well as the water coordinated to copper complexes. The *exothermic* weight losses in the temperature range 523–663 K are attributed to decomposition and combustion of acetato or chloroacetato ligands with different modes of coordination. The decomposition of encapsulated acetato groups bridging two Cu(II) ions in dimeric CuAc molecule occurs around 593 K. For neat dimeric CuAc this decomposition takes place at a lower temperature (~533 K), indicating that the thermal stability of CuAc increases upon encapsulation in zeolites. The exothermic weight loss (~4.5%) around 663 K is attributed to the combustion of acetato groups with a chelate mode of coordination to the zeolite framework or to monomeric Cu(II) complexes.

Chlorine substitution affects the TGA and DTA profiles of both neat and encapsulated CuClAc complexes. Dimeric CuClAc in zeolite-Y decomposes at 538 K compared to 593 K for encapsulated CuAc. An increased thermal stability (by ~40 K) is also observed for CuClAc upon encapsulation. The thermogravimetric data as well as the carbon and hydrogen analysis of the samples confirm the stoichiometric integrity of the encapsulated complexes.

FT-IR Spectroscopy

Indications for the formation of dimeric Cu(II) acetato and monochloroacetato complexes in the supercages of zeolite-Y come from FT-IR spectroscopy (Fig. 2). Selected vibrational band positions for neat and encapsulated CuAc and CuClAc complexes are listed in Table 1. Significant shifts are observed in band positions upon encapsulation. The band for $\nu_{as}(COO^-)$ shifts by ~13 cm^{-1} toward higher energy for CuAc-Y and by ~19 cm^{-1} for CuClAc-Y; similarly, $\nu_s(COO^-)$ shifts by ~19 cm^{-1} toward lower energy

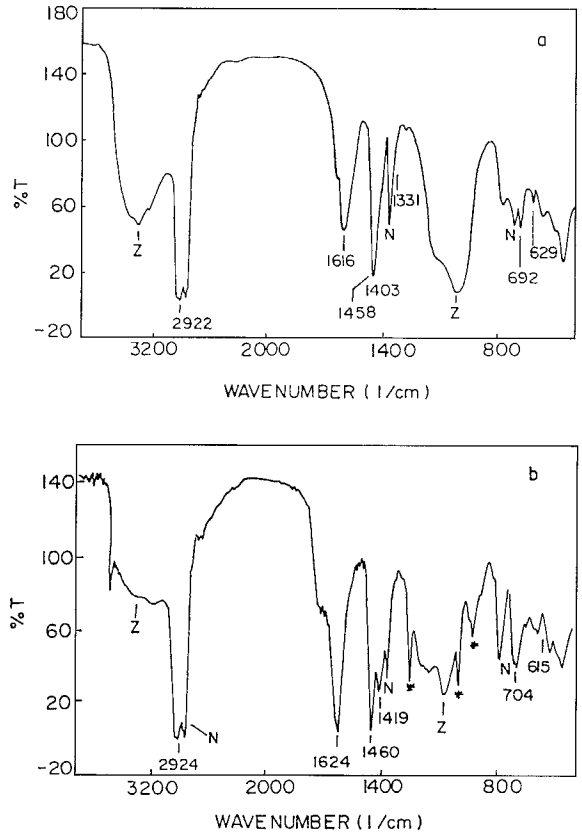

FIG. 2. FT-IR spectra of (a) CuAc-Y and (b) CuClAc-Y as nujol mulls. The band positions of the dimeric complexes are numbered. * = the bands due to the organics in zeolite; N = the bands due to nujol, and Z = the bands due to zeolite-Y.

for CuAc-Y while the position of this band is unaltered for CuClAc-Y. The band at 692 cm^{-1}, corresponding to the deformation of COO^-, is unaltered for CuAc-Y. For CuClAc-Y it is shifted by 10 cm^{-1}. The separation ($\Delta\nu$) between the $\nu_s(COO^-)$ and $\nu_{as}(COO^-)$ bands, indicative of the type of coordination of the carboxylato group, falls well within the range reported for the *syn–syn* mode of

TABLE 1

FT-IR Assignments for "Neat" and Encapsulated Cu(acetato) and Cu(chloroacetato) Dimers

	CuAc		CuClAc	
Assignment	Neat (cm^{-1})	Encapsulated (cm^{-1})	Neat (cm^{-1})	Encapsulated (cm^{-1})
Asym. and sym. C–H stretch	2924	2922	2922	2924
COO^- asym. stretch	1603	1616	1605	1624
COO^- sym. stretch	1421	1403	1420	1419
CH bending	1355	1331	1448	1460
(CH_3, CH_2Cl)	1456	1458		
COO^- deform.	628	629	628	615
	692	692	694	704

coordination (17), but its value increases upon encapsulation (from 182 to 213 cm^{-1} for CuAc and from 185 to 205 cm^{-1} for CuClAc). The FT-IR spectra, thus, indicate that encapsulation results in structural and electronic changes in the carboxylato ligands of the copper complexes.

EPR studies (*vide infra*) indicate that the amount of encapsulated dimeric copper ions is lower in the case of CuClAc than CuAc. However, the larger amount of organic content in CuClAc-Y as seen from the FT-IR spectra (Fig. 2b) and the decomposition profiles in the thermographs (Fig. 1) indicate the presence of additional acetato or chloroacetato ligands/acetic acid molecules in the zeolite. These are presumably chemisorbed on the zeolite surface.

Electronic Spectroscopy

Diffuse reflectance, UV–visible spectra of CuAc and CuClAc showed two characteristic bands, one in the ultraviolet region (band I) and the other in the visible and near-IR region (band II). Band I for neat CuAc and CuClAc occurs at 386 and 377 nm, respectively. For encapsulated complexes, this band shifts to 373 nm (for CuAc-Y) and 387 nm (for CuClAc-Y), respectively. Band II is, in general, broad and unresolved. It occurs in the region 500–900 nm with maxima at 713 and 856 nm for CuAc and CuClAc, respectively. Upon encapsulation these maxima shift to 717 nm (CuAc-Y) and 710 nm (CuClAc-Y), respectively. Thermal analysis, FT-IR spectroscopy, and UV–vis spectroscopy, hence, indicate that the copper complexes undergo significant structural changes upon encapsulation. These changes are investigated in some detail by EPR spectroscopy.

EPR Spectroscopy

Dimeric copper acetate is one of the smallest clusters studied by EPR spectroscopy as early as 1952 by Bleaney and Bowers (18) and subsequently by Abe and Shimada (19). Copper acetate, in the solid state, exists as isolated dimers. The spins on the two copper centers couple antiferromagetically, resulting in a ground-state singlet ($S=0$) and low-lying excited triplet states ($S=1$). At ambient temperatures, the excited triplet state is populated and the complex exhibits paramagnetism (1.4 B.M.). As the temperature is lowered, the excited triplet states are depopulated and, as a consequence, the magnetic moment and EPR signal intensity decrease. Around 20 K the compound is diamagnetic and EPR silent. In the present study, we investigate the influence of chlorine substitution and encapsulation in the zeolite on the structure of the copper dimers using EPR spectroscopy.

EPR of Neat CuAc and CuClAc Complexes

The powder samples of Cu(II) acetato and monochloroacetato complexes showed three EPR signals, at X-band frequency (3-cm wavelength), near 240, 4600, and 5900 G, respectively. The spectra are quite incompatible with spin $S=\frac{1}{2}$ for Cu(II), but could be fitted satisfactorily using the interactive spin Hamiltonian (22, 23) for isolated Cu(II) dimers ($S=1$).

$$\mathcal{H} = DS_z^2 + E\left(S_x^2 - S_y^2\right) + \beta(g_z H_z S_z + g_x H_x S_x + g_y H_y S_y). \quad [1]$$

Here, D and E are the zero-field splitting parameters, β is the Bohr magneton, and x, y, and z are a principal axes coordinating system, fixed with respect to the Cu–Cu bond. When the external magnetic field is in an arbitrary direction with respect to x, y, and z axes, we expect, in general, three transitions: two $\Delta M_s = \pm 1$ transitions and one $\Delta M_s = \pm 2$ transition. When the magnetic field is along x, y, and z directions, respectively, we obtain from Eq. [1] the six $\Delta M_s = \pm 1$ resonance fields,

$$\begin{aligned}
H_{x1}^2 &= (g_e/g_x)^2[(H_0 - D' + E')(H_0 + 2E')],\\
H_{x2}^2 &= (g_e/g_x)^2[(H_0 + D' - E')(H_0 - 2E')],\\
H_{y1}^2 &= (g_e/g_y)^2[(H_0 - D' - E')(H_0 - 2E')],\\
H_{y2}^2 &= (g_e/g_y)^2[(H_0 + D' + E')(H_0 + 2E')],\\
H_{z1}^2 &= (g_e/g_z)^2[(H_0 - D')^2 - E'^2],\\
H_{z2}^2 &= (g_e/g_z)^2[(H_0 + D')^2 - E'^2],
\end{aligned} \quad [2]$$

where $H_0 = h\nu/g_e\beta$, $D' = D/g_e\beta$, and $E' = E/g_e\beta$. H_{z1} and H_{z2} are, for example, the two $\Delta M_s = \pm 1$ transitions when the magnetic field is along the z direction; g_e is the free electron g value. However, in the case of powder samples, the spectrum is an average of the spectra corresponding to several possible orientations. Six allowed $\Delta M_s = \pm 1$ transitions along with a half-field ($\Delta M_s = \pm 2$) transition are observed for a rhombic symmetry (i.e., $E \neq 0$). When $D < h\nu$, four $\Delta M_s = \pm 1$ transitions along with a half-field ($\Delta M_s = \pm 2$) transition are allowed for an axial symmetry ($E = 0$). When $D > h\nu$, as is the case for the present copper dimers, H_{x1} and H_{y1} and the half-field $\Delta M_s = \pm 2$ transition lines can no longer be observed. Hence, the powder spectrum consists of only four lines. If, in addition, $E = 0$, only three EPR lines are observed and Eq. [2] can be rewritten as

$$\begin{aligned}
H_\perp^2 &= (g_e/g_\perp)^2[H_0(H_0 + D')],\\
H_{z1} &= -(g_e/g_z)(H_0 - D'),\\
H_{z2} &= (g_e/g_z)(H_0 + D').
\end{aligned} \quad [3]$$

Representative spectra for neat CuAc and CuClAc are shown in Figs. 3a and 3b and 4a and 4b, respectively. At ambient temperatures, the spectra are more intense and broader (Figs. 3a and 4a). As the temperature is lowered, the intensity decreases and the spectra become narrower and seven hyperfine features, with a relative intensity ratio of 1:2:3:4:3:2:1 due to two interacting Cu(II) ions

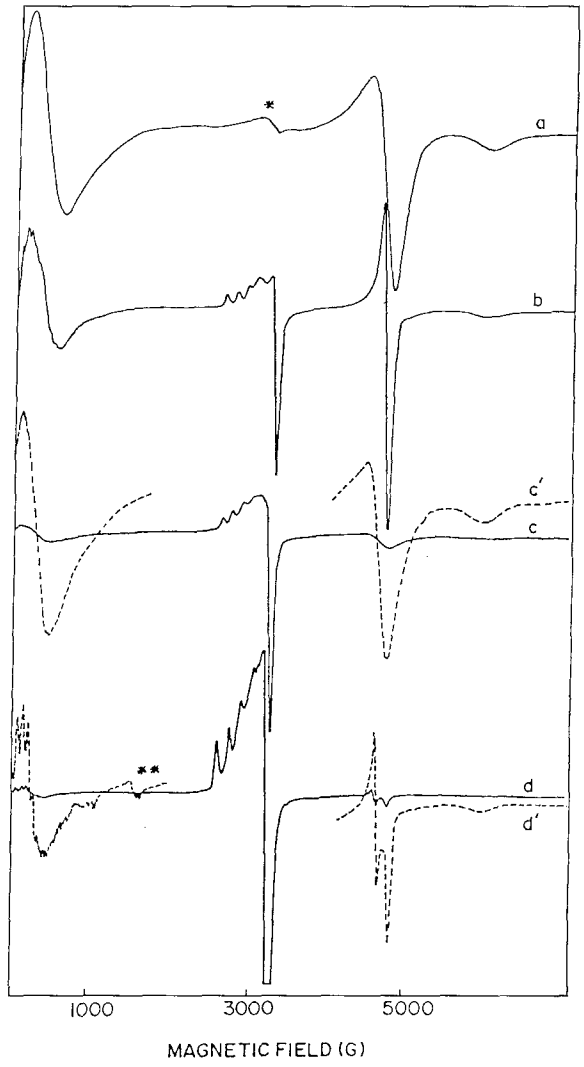

FIG. 3. X-band EPR spectra of "neat" CuAc at (a) 298 K and (b) 95 K and CuAc encapsulated in zeolite-Y at (c) 298 K and (d) 86 K. Signals in dotted lines (c′ and d′) are the dimer signals at higher spectrometer gain. Asterisk (*) indicates signals due to monomeric impurity and ** indicates the Fe(III) impurity in zeolite-Y.

$(2nI+1; n=2$ and $I=\frac{3}{2})$, are observed on the low-field signal (Figs. 3b and 4b). An expanded portion of the spectrum in the low-field region revealing the septet hyperfine pattern is shown in Fig. 5. The effect of substitution (by Cl) is more evident in the low-temperature spectra around 4800 G (see Figs. 3b and 4b). While the spectra for CuAc could be fitted with a rhombic spin Hamiltonian ($E \neq 0$ and $g_x \neq g_y$), that of CuClAc could be fitted only with an axial spin Hamiltonian ($E \approx 0$). In other words, the symmetry around Cu is C_{4v} for neat CuClAc and C_{2v} for CuAc. This difference in the molecular symmetry of neat CuClAc and CuAc is attributed to a difference in the carboxylato ion binding. This inference from EPR study agrees well with the X-ray structure of neat CuAc (13, 14). According to the latter, the *cis*-carboxylato groups bind differently to the central metal ion Cu(II), the average *cis*-C–O bond distances are 1.990 and 1.948 Å, respectively, and the basal CuO_4 is nonplanar and results in an overall C_{2v} symmetry at the individual copper atoms of the dimer. The EPR parameters for neat CuAc and CuClAc, obtained after least-squares fitting to the Eqs. [2] and [3], respectively, are listed in Table 2.

EPR of CuAc-Y and CuClAc-Y

Typical spectra for neat CuAc and CuAc-Y as well as CuClAc and CuClAc-Y are shown in Figs. 3 and 4, respectively. The spin Hamiltonian parameters obtained after fitting the spectra to Eq. [2] are listed in Table 2 along with the values for the neat complexes. Curves b in Figs. 3 and 4 represent the EPR spectra at 95 K of neat CuAc and neat CuClAc,

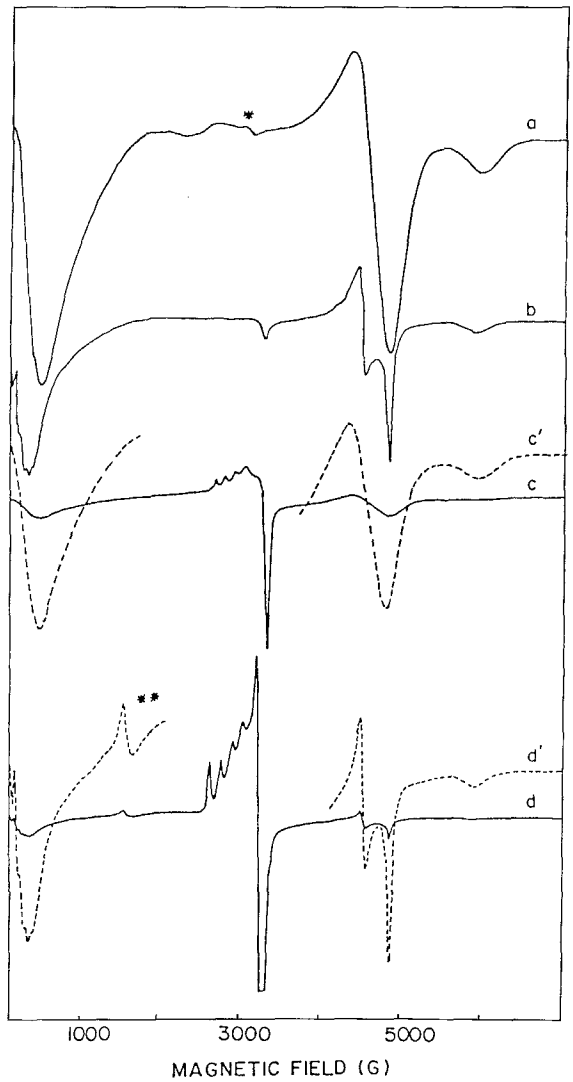

FIG. 4. X-band EPR spectra of "neat" CuClAc at (a) 298 K and (b) 80 K and CuClAc encapsulated in zeolite-Y at (c) 298 K and (d) 80 K. Signals in dotted lines (c′ and d′) are the dimer signals at higher spectrometer gain. Asterisk (*) indicates the signals due to monomer impurity and ** indicates the Fe(III) impurity in zeolite-Y.

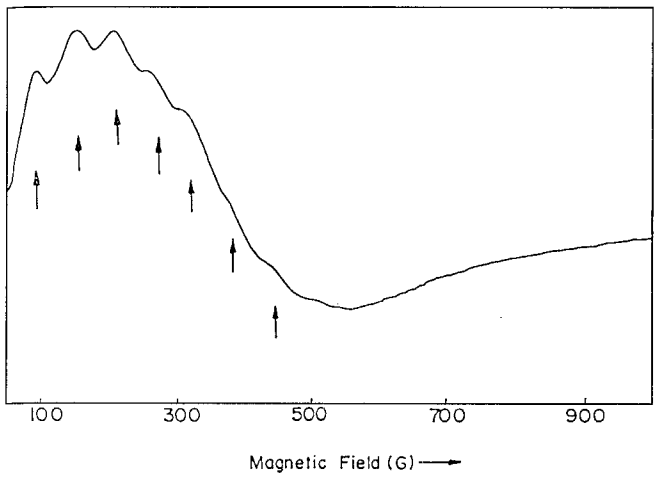

FIG. 5. Expanded portion of the dimer signal near zero magnetic field showing the hyperfine resolution due to two interacting copper ions in "neat" CuClAc.

respectively. They are different because of the different symmetries of the Cu(II) ions in the two cases (C_{2v} for CuAc and C_{4v} for CuClAc). Their EPR spin Hamiltonian and structural parameters are, hence, different (see Table 2). Curves d in Figs. 3 and 4 represent the EPR spectra (at 80–86 K) of CuAc and CuClAc, respectively, encapsulated in zeolite-Y. The differences between curves b and d in Fig. 3 compared to similar differences in Fig. 4 arise primarily because of changes in the symmetry of the Cu(II) ions responsible for curve b (in Fig. 3) and curve b (in Fig. 4). There are significant differences between CuAc-Y (curve d in Fig. 3) and CuClAc-Y (curve d in Fig. 4). This may be seen from the different values of their spin Hamiltonian and structural parameters (Table 2).

Two types of encapsulated Cu(II) species, I and II, may be distinguished; species I is the encapsulated dimeric copper(II) acetato or chloroacetato complex and species II (marked by an asterisk,*) corresponds to monomeric Cu(II) ions. A comparison of the spectrum for species II with that of Cu–H-Y containing a lower amount of Cu (0.011 wt%) indicates that the Cu(II) ions of species II are located in the sodalite cages of zeolite-Y. The Cu(II) ions in the sodalite cages do not form copper–copper dimeric complexes with acetic acid or chloroacetic acid due to the geometric constraints in the sodalite cages. No apparent difference is observed in the spectra of CuAc upon encapsulation (see Figs. 3a and 3c and Figs. 3b and 3d). CuClAc, on the other hand, shows marked changes upon encapsulation (Figs. 4a and 4c and Figs. 4b and 4d). CuClAc, which exhibits an axial spectrum in the neat state, corresponding to a C_{4v} symmetry (Fig. 4, curve b) exhibits a rhombic-type spectrum corresponding to a C_{2v} symmetry after encapsulation (Fig. 4, curve d) (see the splitting of the signal around 4800 G upon encapsulation). A higher resolution of the copper hyperfine lines is also observed on the signal near 240 G (Fig. 4, curve d). From a comparison of the signal intensities of the dimeric neat and encapsulated complexes, the amounts of acetato and chloroacetato complexes encapsulated in the supercages were estimated to be 65% and 20% (of the total copper) for CuAc and CuClAc, respectively. The remaining copper is located, mostly, in the sodalite cages. In Cu–H-Y, the copper ions in the sodalite cage show rhombic EPR spectra at 298 K ($g_z = 2.376$, $g_x = 2.083$, $g_y = 2.095$, $A_z = 119$ G, $A_x = A_y = 10$ G). Above 275 K, the Cu(II) ions in the supercages and those near the hexagonal prism (in Cu–H-Y) exhibit a broad isotropic spectrum ($g_{iso} = 2.194$, $\Delta H_{pp} = 175$ G). Below 275 K, the spectrum becomes axial ($g_\parallel = 2.392$, $g_\perp = 2.093$, $A_\parallel = 132.2$ G, and $A_\perp = 25$ G). The reason for this transition is the Jahn Teller distortions of the Cu(II) ions in the supercages or those near the hexagonal prism with O_h/D_{3h} symmetry (20). These signals due to Cu(II) ions in the supercage and near the hexagonal prism are not present in CuAc-Y and CuClAc-Y; instead, new signals due to dimeric acetato and chloroacetato complexes appear (Figs. 3 and 4, respectively), confirming the formation of the dimeric complexes and their location in the supercages. From the EPR signal intensity and thermogravimetric data we estimate that, on an average, the copper dimers occupy one in two (CuAc-Y) or one in eight (CuClAc-Y) of the supercages of the faujasite lattice.

At high temperatures, the triplet states are relatively more populated and the dimer signals are broader due to short, electron spin-lattice relaxation times (T_{1e}) and intermolecular interactions. As the temperature is lowered, the excited triplet levels are depopulated and the copper hyperfine features are better resolved. The intensity of the signal of a monomeric paramagnetic ion, obeying the Curie–Weiss

TABLE 2

EPR Spin Hamiltonian and Structural Parameters of "Neat" and Encapsulated CuAc and CuClAc

Complex	g_z	g_x	g_y	A(Cu) (cm^{-1})	D (cm^{-1})	E (cm^{-1})	$-J$ (cm^{-1})	Cu–Cu r (Å)
CuClAc ("neat")	2.348	2.068	2.068	0.0054	0.34	0.0	247	2.92
CuClAc-Y	2.353	2.064	2.070	0.0066	0.34	0.03	132	2.73
CuAc ("neat")	2.358	2.055	2.095	0.0073	0.34	0.07	259	2.64
CuAc-Y	2.358	2.055	2.095	0.0073	0.34	0.07	310	2.40

law, is inversely proportional to the temperature. The ratio (R) of the intensity of the dimer (I_{dimer}) to that of the monomer ($I_{monomer}$) signals is

$$R = 2\exp(-J/kT)/[1 + 3\exp(-J/kT)]. \quad [4]$$

The signal of Cu–H-Y was taken as the reference paramagnetic ion signal. In Eq. [4], J is the exchange coupling constant or singlet–triplet separation. Its sign is negative for antiferromagnetic interaction and positive for ferromagnetic interaction. The plots of relative intensities (R) of dimer-to-monomer signals for CuAc and CuClAc, before and after encapsulation, are depicted in Fig. 6. If the triplet levels are not very much higher in energy than the singlet or if the magnitude of J is small, then $-\log R$ should increase linearly with T^{-1}. Such a behaviour is indeed observed for CuClAc complexes (Fig. 6, curve b). The plots for CuAc and CuAc-Y, on the other hand, are linear only up to a certain temperature (210 and 160 K, for the neat and encapsulated complexes, respectively, Fig. 6, curve a). The relative intensity values (R) were fitted to Eq. [4] and the exchange coupling constant (J) were obtained for both neat and encapsulated complexes (Table 2). The value of J for CuAc ($-259\ cm^{-1}$) compares well with that reported by Bleaney and Bowers (18) and to that obtained by bulk susceptibility measurements ($-286\ cm^{-1}$) (21). From Table 2, we may infer the following consequences of substitution and encapsulation.

(1) The g values ($g_z > g_x$ and g_y) reveal a tetragonal distortion of the molecular geometry around Cu(II) and indicate that the unpaired electron occupies a "formal" $3d_{x^2-y^2}$ orbital of Cu(II).

(2) The electron-withdrawing Cl substitution significantly influences the symmetry of the g and zero-field tensors. Their values are characteristic of a rhombic symmetry for the neat acetato complex and an axial symmetry for the neat chloroacetato complex. Chlorine substitution alters the magnitude of the exchange coupling constant

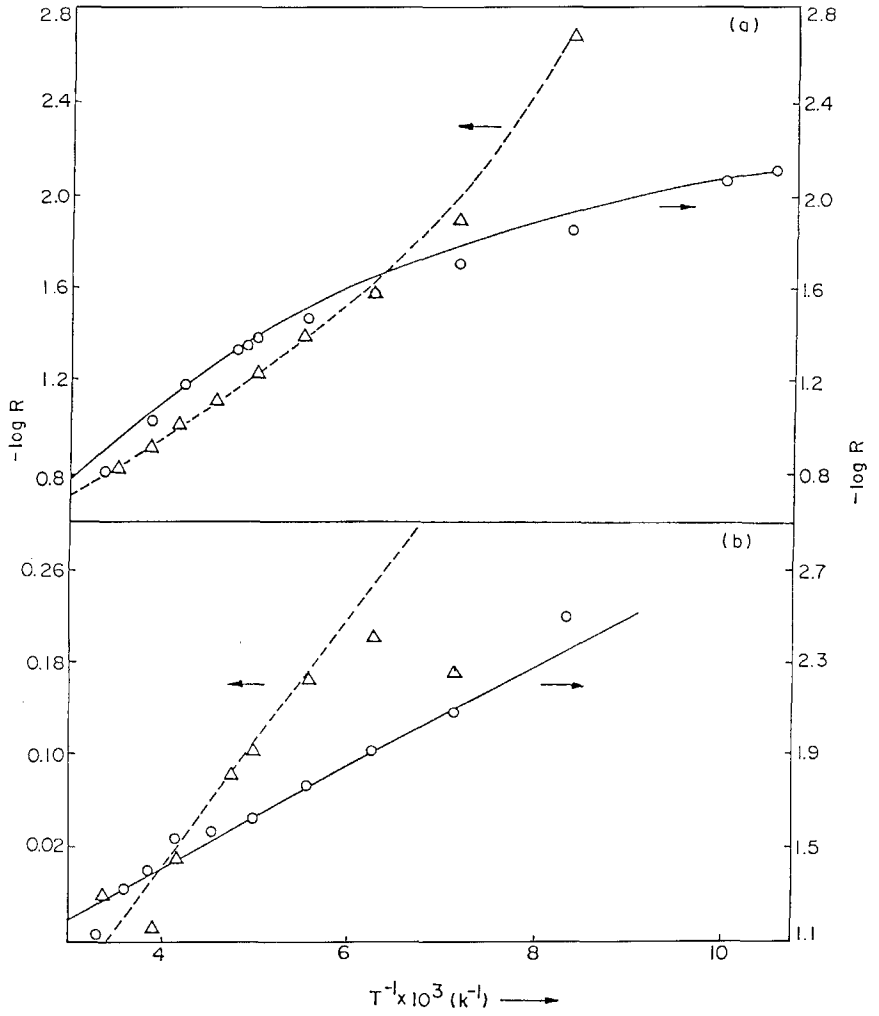

FIG. 6. Plot of log R vs T^{-1} for "neat" (—) and encapsulated (- - -) complexes of (a) CuAc and (b) CuClAc.

(J changes from $-259\ cm^{-1}$ for CuAc to $-247\ cm^{-1}$ for CuClAc).

(3) The value of A(Cu) is smaller for CuClAc ($54 \times 10^{-4}\ cm^{-1}$) than for CuAc ($73 \times 10^{-4}\ cm^{-1}$), consistent with a depletion of electron density from Cu orbitals on chlorine substitution.

(4) The molecular symmetry at copper in CuClAc reduces from C_{4v} to a lower symmetry (C_{2v}) as a consequence of encapsulation. CuAc has a lower symmetry in both the neat and encapsulated complexes.

(5) An increase in the value of a copper hyperfine coupling constant (from 54×10^{-4} to $66 \times 10^{-4}\ cm^{-1}$) is observed for CuClAc upon encapsulation, probably due to changes in the molecular geometry of CuClAc, caused by confinement and consequent host–guest interactions in the supercages. Such a change (in A values) is not observed for the CuAc complex, probably due to its smaller size.

(6) The value of J is negative for both CuAc and CuClAc, indicating that the Cu–Cu interactions are antiferromagnetic. Interestingly, the exchange coupling constant ($-J$) increases from 259 to $310\ cm^{-1}$ upon encapsulation for CuAc. But it decreases from 247 to $132\ cm^{-1}$ for CuClAc upon encapsulation.

The zero-field splitting parameter (D_{total}), obtained from experiment, has contributions from exchange and direct dipole–dipole interactions (22, 23), i.e.,

$$D_{total} = D_{ex} + D_{dip}. \quad [5]$$

Considering, for the sake of simplicity, an axial symmetry for both CuAc and CuClAc, the D_{ex} and D_{dip} terms can be related to the exchange coupling constant (J) and internuclear Cu–Cu separation (r) as follows:

$$D_{ex} = -(J/8)[(g_{\parallel} - 2)^2/4 - (g_{\perp} - 2)^2], \quad [6]$$

$$D_{dip} = -[g_{\parallel}^2 + (1/2)g_{\perp}^2]\beta^2/r^3. \quad [7]$$

Here, $g_{\parallel} = g_z$ and $g_{\perp} = (g_x + g_y)/2$. Interestingly, electron-withdrawing substituents and encapsulation have only a minor effect on D_{toal} values while marked changes are observed in the values of J, the exchange coupling constants (24). The intramolecular Cu–Cu separation (r), estimated from Eqs. [5]–[7] by substituting the values of g and J, are given in Table 2. This value of r is larger for CuClAc than for CuAc and it decreases upon encapsulation for both CuAc and CuClAc from 2.64 to 2.40 Å and 2.92 to 2.73 Å, respectively. The value of 2.64 Å for neat CuAc matches well with that reported from X-ray diffraction (2.61 Å) and validates the Cu–Cu distances estimated from EPR spectroscopy. Conventional X-ray diffraction methods cannot be used to estimate such intermolecular distances in encapsulated complexes (13, 14). Although there may be some error in the estimation of the Cu–Cu separation, arising from the assumption of axial instead of rhombic symmetry, the reduction of r by about 0.2 Å due to encapsulation is a significant feature and indicates changes in the coordination/conformation of the carboxylato group. The shifts, upon encapsulation, in the IR band positions of $\nu_{as}(COO^-)$ and $\nu_s(COO^-)$ and the UV band near 375 nm, all characteristic of the carboxylato bridge, also support such an inference.

To summarize, the spectroscopic and thermogravimetric studies reveal that the dimeric acetato and chloroacetato complexes of Cu(II) are encapsulated in the supercages of zeolite-Y. The dimensions of these dimeric Cu(II) complexes are more than 8.5×10 Å while the size of the window for the supercage is only about 7.4 Å. Hence, these complexes, once formed, are truly encapsulated and cannot come out of the supercages of zeolite-Y easily. Encapsulation has a significant effect on the molecular and electronic structure of CuAc and CuClAc as revealed by EPR. The CuAc has a lower symmetry (C_{2v}) in both neat and encapsulated complexes. On the other hand, the symmetry of Cu(II) ions in CuClAc changes from C_{4v} to C_{2v} upon encapsulation. This lowering of symmetry for CuClAc is probably due to the greater geometric constraints on the larger CuClAc dimeric complexes upon encapsulation. In addition to the changes in the molecular symmetry, the Cu–Cu separation decreases by about 0.2 Å for both the complexes as a consequence of encapsulation.

Catalytic Activity of CuAc-Y and CuClAc-Y

The catalytic activities of CuAc and CuClAc in the oxidation of phenol to *o*-benzoquinone are compared in Table 3. The following features are noted:

(1) Hydroxylation does not occur in the absence of the catalyst.

(2) Both CuAc-Y and CuClAc-Y oxidize phenol selectively to *o*-benzoquinone.

(3) The turnover frequency for oxidation is enhanced significantly upon encapsulation of the complexes in zeolite-Y for both CuAc and CuClAc.

(4) The specific catalytic activity (turnover frequency) of CuClAc-Y is higher than that of CuAc-Y at similar levels of phenol conversion.

TABLE 3

Hydroxylation of Phenol Using Molecular Dioxygen as the Oxidant (pH 6.5, Temp. = 298 K, Reaction Time = 19 h)

Catalyst	Phenol conv. (mol%)	BzQ (mol%)	Others (mol%)	TOF (h^{-1})
CuAc "neat"	5.1	4.9	0.2	3.6
CuAc-Y	11.5	11.5		60.9
CuClAc "neat"	1.0	1.0		0.9
CuClAc-Y	12.0	11.9	0.1	227.1

TON = turnover frequency (number of molecules of phenol converted per atom of Cu per hour).

CuAc complexes mimic, functionally, the enzymatic activity of the copper monooxygenase enzyme, tyrosinase, in the regiospecific *o*-hydroxylation of phenols to catechols and further oxidation of catechol to *o*-benzoquinone (11, 12). Interestingly, this enzyme also contains a dicopper site as the active center. The proposed mechanism (15) for tyrosinase involves dioxygen binding to Cu_2 sites to generate a Cu_2–O_2 side-on bound oxygen adduct (η^2–η^2 type of peroxide coordination). During the hydroxylation reaction, the tyrosine phenolate group coordinates directly to Cu(II) ion, leading to donation of electron density from the substrate tyrosine to the LUMO of the complex which is antibonding with respect to both the O–O and Cu–O bonds. This electron transfer, in turn, initiates the transfer of one of the two peroxide oxygens to the position ortho to the OH group in the tyrosine molecule. The resultant coordinated catecholate ion will transfer two electrons to the binuclear cupric ion, leading to the dissociative elimination of the product and the regeneration of the deoxy site for further turnover. It is pertinent to note that the EPR spectra of phenol adsorbed on the encapsulated CuAc complexes in the presence of O_2 give clear evidence for the formation of an axially coordinated copper–phenol adduct (25), an intermediate identified during the oxidation of phenols by tyrosinase. The labile coordination of the axial ligand (phenol, in our case) and the enhanced catalytic activity of the encapsulated dimeric copper acetate could both be attributed, perhaps, to the shorter Cu–Cu distance and consequent greater interaction between the two copper ions in the encapsulated state compared to the neat complex. The short Cu–Cu distance and the consequent greater, lateral, overlap of the copper orbitals would facilitate the transfer of electron density from the phenolate ligand to the antibonding LUMO of the complex, thereby weakening the O–O and Cu–O bonds. Weakening of these bonds would, in turn, make it easier for the cleavage and the transfer of one of the two oxygens of the peroxide ligand to the position ortho to the phenolate bond. Analogous rhodium complexes having direct overlap of the metal orbitals also exhibit such trans axial lability and consequent enhanced catalytic activity (26). In quadruply bridged dinuclear platinum clusters, with a "lantern-type" structure similar to copper acetate, a strengthening of the metal–metal bond often leads to a decrease in the strength of the metal–axial ligand bond (27).

A qualitative and preliminary picture (Scheme 1) of the mechanism of oxidation that emerges from our studies is the following: Under the reaction conditions (pH 6.5) (28), the phenols exist in the phenolate form. Two phenolate ions coordinate to the two Cu(II) ions of the copper acetate dimer, reducing them to the Cu(I) oxidation state.

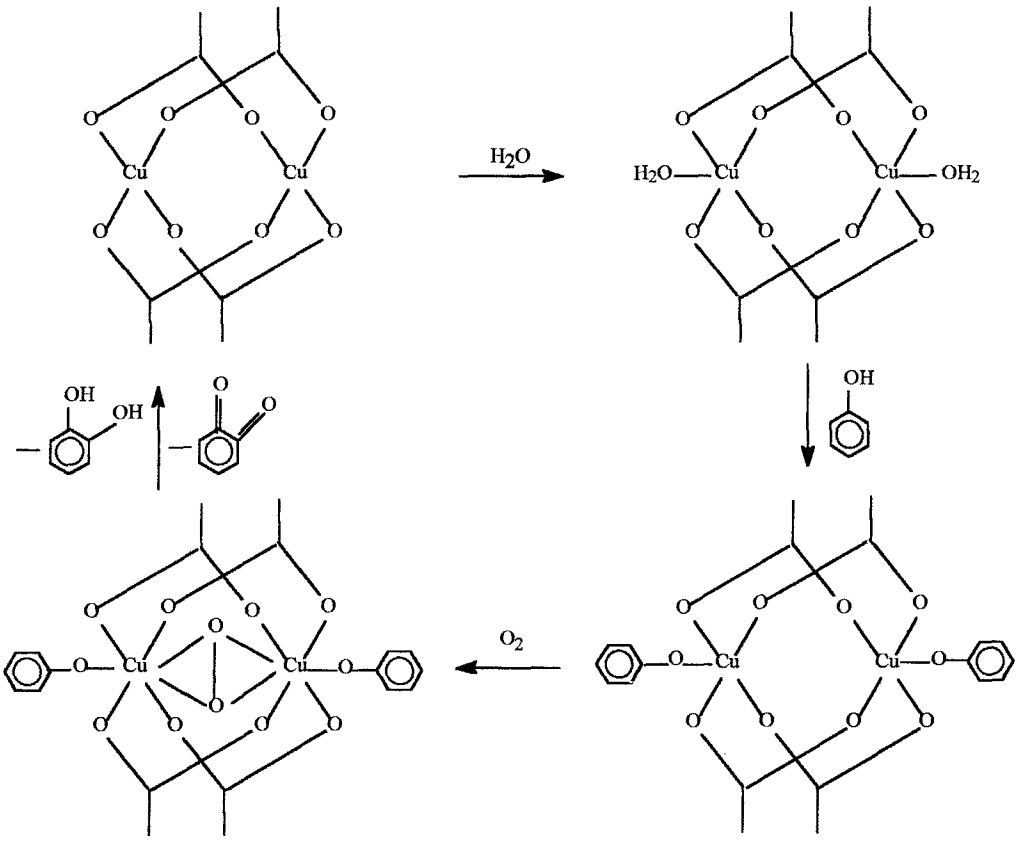

SCHEME 1

Next, dioxygen reacts with the copper–phenolate complex, forming a Cu_2–O_2–phenolate adduct. The latter undergoes a O–O bond scission concomitant with the hydroxylation of the substrate. The acetate group can change its mode of coordination from a bidentate to a monodentate type as a consequence of forming the dioxygen adduct. Such a coordination lability is common in the enzymatic reactions.

CONCLUSIONS

We have investigated the cause of the enhancement in the catalytic activity of dimeric copper acetate and copper chloroacetate complexes in the *o*-hydroxylation of phenols when encapsulated in zeolite-Y. EPR spectra confirm the location of these complexes in the supercages of the zeolite. Even though the stoichiometric integrity of the complex is conserved upon encapsulation, the shift in the vibrational and electronic band positions clearly reveal changes in the carboxylate bridge coordination. The variation in the EPR spectral intensities in the range of 77–298 K indicates that the Cu–Cu antiferromagnetic exchange interaction increases upon encapsulation due to the compression of the Cu–Cu separation to 2.40 Å from 2.64 Å for the neat copper acetate complex. The corresponding decrease for CuClAc is from 2.92 Å (neat) to 2.73 Å (encapsulated). Geometric constraints imposed by the cavities of the zeolite probably cause the observed geometric changes in the structure of these encapsulated complexes. Due to the greater Cu–Cu bonding, the strength and the lability of the Cu–phenolate and Cu–dioxygen bonds are modified by a trans axial ligand effect, leading to enhanced reactivity of the encapsulated complex. There is, hence, a direct, causal relationship between the shortening of the internuclear Cu–Cu distance upon encapsulation and the enhanced reactivity of the resultant, structurally modified complex. The geometric (and the consequent electronic) changes are probably at the origin of the enhanced catalytic activity of the encapsulated complexes. Hence, by varying the substituent groups on the acetate ligand and the shape and size of the zeolite cavity, one should be able, at least in principle, to design suitable solid catalysts for selective oxidation reactions at low temperatures in the liquid phase.

ACKNOWLEDGMENT

The authors thank Dr. (Mrs.) S. Deogaonkar and Dr. (Mrs.) Nalini E. Jacob for their help in this work.

REFERENCES

1. Balkus, K. J., Jr., and Gabrielov, A. G., *J. Incl. Phenom. Mol. Recog. Chem.* **21**, 159 (1995).
2. Balkus, K. J., Jr., Gabrielov, A. G., and Bell, S. L., *Inorg. Chem.* **33**, 67 (1994).
3. Herron, N., *CHEMTECH* **19**, 542 (1989).
4. Holland, B. T., Walkup, C., and Stein, A., *J. Phys. Chem. B* **102**, 4301 (1998).
5. Bowers, C., and Dutta, P. K., *J. Catal.* **122**, 271 (1990).
6. Parton, R. F., Bezoukheanova, C. P., Grobet, J., Grobet, P. J., and Jacobs, P. A., *Stud. Surf. Sci. Catal.* **83**, 371 (1994).
7. Raja, R., and Ratnasamy, P., *Appl. Catal. A* **158**, L7 (1997).
8. Jacob, C. R., Varkey, S. P., and Ratnasamy, P., *Appl. Catal. A* **168**, 353 (1998).
9. Jacob, C. R., Varkey, S. P., and Ratnasamy, P., *Microporous Mesoporous Mater.* **22**, 465 (1998).
10. Raja, R., and Ratnasamy, P., *Catal. Lett.* **48**, 1 (1998).
11. Raja, R., and Ratnasamy, P., *J. Mol. Catal. A* **100**, 93 (1995).
12. Eswaramoorthy, M., Neeraj, and Rao, C. N. R., *J. Chem. Soc. Chem. Commun.* 615 (1998).
13. Van Niekerk, J. N., and Schoening, F. R. L., *Acta Crystallogr.* **6**, 227 (1953).
14. de Meester, P., Fletcher, R., and Skapski, A. C., *J. Chem. Soc. Dalton Trans.* 2575 (1973).
15. Solomon, E. I., and Lowery, M. D., *Science* **259**, 1575 (1993).
16. Solomon, E. I., Tuczek, F., Root, D. E., and Brown, C. A., *Chem. Rev.* **94**, 827 (1994).
17. Mehrotra, R. C., and Bohra, R., "Metal Carboxylates." Academic Press, New York (1983).
18. Bleaney, B., and Bowers, K. D., *Proc. R. Soc. London A* **214**, 451 (1952).
19. Abe, H., and Shimada, J., *Phys. Rev.* **90**, 316 (1953).
20. Naccache, C., and Ben Taarit, Y., *Chem. Phys. Lett.* **11**, 11 (1971).
21. Figgis, B. N., and Martin, R. L., *J. Chem. Soc.* 3837 (1956).
22. Smith, T. D., and Pilbrow, J. R., *Coord. Chem. Rev.* **13**, 173 (1974).
23. Bertini, A., and Gatteschi, D., "EPR of Exchange Coupled Systems," Chap. 10. Springer Verlag, Berlin, 1990.
24. Melnik, M., *Coord. Chem. Rev.* **36**, 1 (1991).
25. Chavan, S., Srinivas, D., and Ratnasamy, P., unpublished results.
26. Felthouse, T. R., *Prog. Inorg. Chem.* **29**, 73 (1982).
27. Umakoshi, K., and Sasaki, Y., *Adv. Inorg. Chem.* **40**, 187 (1993).
28. Thomas, J. M., *Nature* **368**, 289 (1994).